J Mater Sci (2010) 45:4583–4593
DOI 10.1007/s10853-010-4420-9

ULTRAFINE GRAINED MATERIALS

Effect of strain reversals on the processing of high-purity aluminum by high-pressure torsion

Megumi Kawasaki · Byungmin Ahn · Terence G. Langdon

Received: 13 February 2010 / Accepted: 15 March 2010 / Published online: 30 March 2010

Abstract High-purity aluminum was processed by high-pressure torsion (HPT) under conventional monotonic (m-HPT) and cyclic (c-HPT) conditions where strain reversals are introduced in c-HPT during processing. Measurements show higher values of the Vickers microhardness in the center regions of all disks but these values are higher when processing by c-HPT by comparison with m-HPT for the same total number of turns. Slightly smaller grain sizes are observed in the c-HPT samples. It is shown that all of the microhardness values correlate with the estimated values of the equivalent strain and the results are consistent with earlier data reported under c-HPT conditions when it is recognized that the variation of hardness with equivalent strain is dependent upon the level of recovery within the material.

Introduction

The processing of metals through the application of severe plastic deformation provides an opportunity for introducing exceptional grain refinement within bulk samples [1]. Several methods are now available for producing ultrafine-grained microstructures [2] but the two procedures receiving most attention are equal-channel angular pressing (ECAP) [3] and high-pressure torsion (HPT) [4].

M. Kawasaki (✉) · B. Ahn · T. G. Langdon
Departments of Aerospace & Mechanical Engineering and Materials Science, University of Southern California, Los Angeles, CA 90089-1453, USA
e-mail: mkawasak@usc.edu

T. G. Langdon
Materials Research Group, School of Engineering Sciences, University of Southampton, Southampton SO17 1BJ, UK

The principle of processing by ECAP was introduced almost 30 years ago by Segal et al. [5]. In practice, ECAP is a discontinuous process because samples, in the form of bars or rods, are pressed repetitively through a die containing a channel where an internal angle is used to impose a high strain. Because the samples are removed from the die between each pass, it is possible to develop different processing routes by rotating the sample between each pass to activate different slip systems [6]. These slip systems have been evaluated [7] and distinct processing routes are now available for the ECAP procedure [8, 9]. Early experiments were conducted to determine the significance of these processing routes using high-purity aluminum [10, 11].

The principles of HPT were first proposed over 70 years ago by Bridgman [12, 13] but the process has received significant attention only within the last 20 years. When a disk is processed in conventional HPT, the equivalent von Mises strain imposed on the disk, ε_{eq}, is given by the relationship [14–16].

$$\varepsilon_{eq} = \frac{2\pi Nr}{h\sqrt{3}} \quad (1)$$

where N is the number of turns, r is the radius, and h is the height (or thickness) of the disk. This relationship shows that the strain reaches a maximum at the edge of the disk but it is reduced to zero in the center of the disk where $r = 0$ mm. It follows that since the material in any position other than the center of the disk receives an equivalent strain by torsion straining, it is possible to estimate the appropriate values of the equivalent strain at any selected position within the disk.

Processing by HPT differs in a significant way from ECAP because it is a continuous process and it consists of taking a sample, typically in the form of a thin disk, and

compressing between heavy anvils with concurrent torsional straining. Since the process is continuous, it is not feasible to develop the various processing routes that have become important in ECAP but instead it is possible to conduct either conventional monotonic testing, termed m-HPT, in which the sample is continuously rotated in the same direction during straining or cyclic testing, termed c-HPT, where the sample is retained within the HPT facility but the direction of straining is periodically reversed at selected strain intervals. The use of c-HPT was first introduced a few years ago in a test on an Al–3%Mg–0.2%Sc alloy [17] and more recently there have been reports of c-HPT experiments on Al [18–21], Fe [22], Ni [22, 23], Pd [24, 25], pearlitic steel [26], and Ti [27]. An earlier report gave details of the application of c-HPT to high-purity Al with an emphasis on optical inspection of the disks after processing to reveal the macroscopic characteristics of the flow behavior [18]. Accordingly, the present investigation was initiated to provide detailed information on the microstructural evolution occurring in high-purity Al during c-HPT by making extensive use of transmission electron microscopy (TEM).

Experimental material and procedures

The investigation was performed using polycrystalline high-purity (99.99%) aluminum. Following the detailed material preparation described earlier [18], an aluminum block with dimensions of ~30 mm diameter and ~150 mm length was swaged at room temperature into a rod having a diameter of 10 mm and the rod was cut into a length of ~60 mm. The rod was annealed at 773 K for 1 h to give an initial grain size of ~1 mm and it was then sliced into disks having thicknesses of ~1.5–2.0 mm. Both sides of these disks were carefully polished using several abrasive papers to give a series of HPT samples with thicknesses of ~0.8 mm.

Processing by HPT was conducted at room temperature using an HPT facility of the type described earlier [18]. The facility consisted of upper and lower anvils with each anvil machined with a flat inner surface on which there was a circular depression, located at the center, having a depth of 0.25 mm and a diameter of 10 mm. The disk sample with a thickness of ~0.8 mm was placed in the depression on the lower anvil and the lower anvil was then brought into position close to the upper anvil so that the disk was contained within the depressions on the two anvil surfaces. All of the processing was conducted using an applied load of ~49 tons which is equivalent to an imposed compression pressure of $P = 6.0$ GPa. Torsional straining was applied by rotating the lower anvil at a constant speed of 1 rpm. Three of the disks were processed using monotonic HPT (m-HPT) in the forward direction through one, two, and four turns, respectively. For cyclic HPT (c-HPT), the two directions of straining were arbitrarily designated A and B. The tests were conducted by rotating through one or two complete turns in the A direction and one or two complete turns in the B direction through the processing routes that are denoted by (1A + 1B), (2A + 2B), and (1A + 1B + 1A + 1B) where these three c-HPT conditions lead to totals of two, four, and four turns, respectively. It should be noted that for tests conducted in c-HPT the direction of torsional straining was changed systematically during the test by stopping the rotation of the lower anvil and then immediately starting rotation again in the opposite direction. This cyclic process of changing the rotational direction was achieved within <2 s.

Following HPT, all disks were mounted and polished carefully to obtain mirror-like surfaces where the revealed clean surfaces were less than ~0.1 mm from the initial surfaces after processing. The values of the Vickers microhardness were then recorded on each disk. These microhardness measurements were conducted using an FM-1e microhardness tester equipped with a Vickers indenter using a load of 100 gf and with a dwelling time for each separate measurement of 15 s. As described earlier [18], the values of the Vickers microhardness, Hv, were measured using two different procedures to obtain the following detailed information on the variations of the hardness values. First, the Hv values were recorded across the diameters of each disk. Second, the distributions of the hardness values were recorded over the total surfaces of each individual disk. For the hardness measurements across the diameters of the disks, the average values of Hv were measured at selected positions from the centers of the disks to both edges where these measurements relate to individual positions separated by incremental distances of 0.3 mm. For each of position, the average value of Hv was determined from four separate hardness measurements recorded at uniformly separated points displaced from the selected point by a distance of 0.15 mm. Using this procedure, it was possible to achieve a very high degree of accuracy in the hardness measurements. For the hardness profiles over the total disk surfaces, the individual values of Hv were recorded following a rectilinear grid pattern with separations of 0.3 mm between each consecutive point. All of these individual values of Hv were then used to construct color-coded three-dimensional mesh plots that gave clear visual presentations of the distributions of local hardness across the surface of each disk.

All disk samples were prepared for microstructural observations and grain size measurements using TEM. The HPT disks were polished from both sides to have thicknesses of ~100 μm using a conventional polishing method without micro-cloths. Disks were punched for TEM at

radial distances from the center, r, of 0 and 3.5 mm and the centers of these TEM disks were thinned using a single-jet electropolishing method with a mixed solution of perchloric acid and ethanol at a temperature close to 273 K. The TEM observations were performed using a Philips EM-420 microscope operating at an accelerating voltage of 120 kV. Average grain sizes were determined directly from the TEM images using separate grain measurements for at least ~300 individual grains.

Experimental results

Microhardness measurements along disk diameters after HPT

The values of the Vickers microhardness, Hv, were measured across the diameters of each separate sample after both m-HPT and c-HPT. To visualize the trends in the hardness values and obtain a more complete understanding of the differences between the m-HPT and the c-HPT samples, it is preferable to plot the data as Hv versus distance across a diameter on each separate disk. Figure 1 shows the experimental data for disks after processing through (a) $N = 1$ turn, (b) $N = 2$ turns including two turns by m-HPT and the 1A + 1B condition using c-HPT, and (c) $N = 4$ turns including four turns by m-HPT and the 2A + 2B and 1A + 1B + 1A + 1B conditions by c-HPT: in each plot the lower solid points denote the hardness values across the disk diameter of the material in the annealed condition without HPT.

Figure 1 shows several general trends that document the hardness evolution after HPT.

First, all of the samples processed by HPT show significantly higher hardness values of >35 across the diameters by comparison with the values of Hv ≈ 20 in the annealed condition prior to HPT. In practice, the hardness after HPT is higher by a factor of ~2 at the edges of the disk between the annealed condition and $N = 1$ turn shown in Fig. 1a but thereafter the hardness values at the edges of

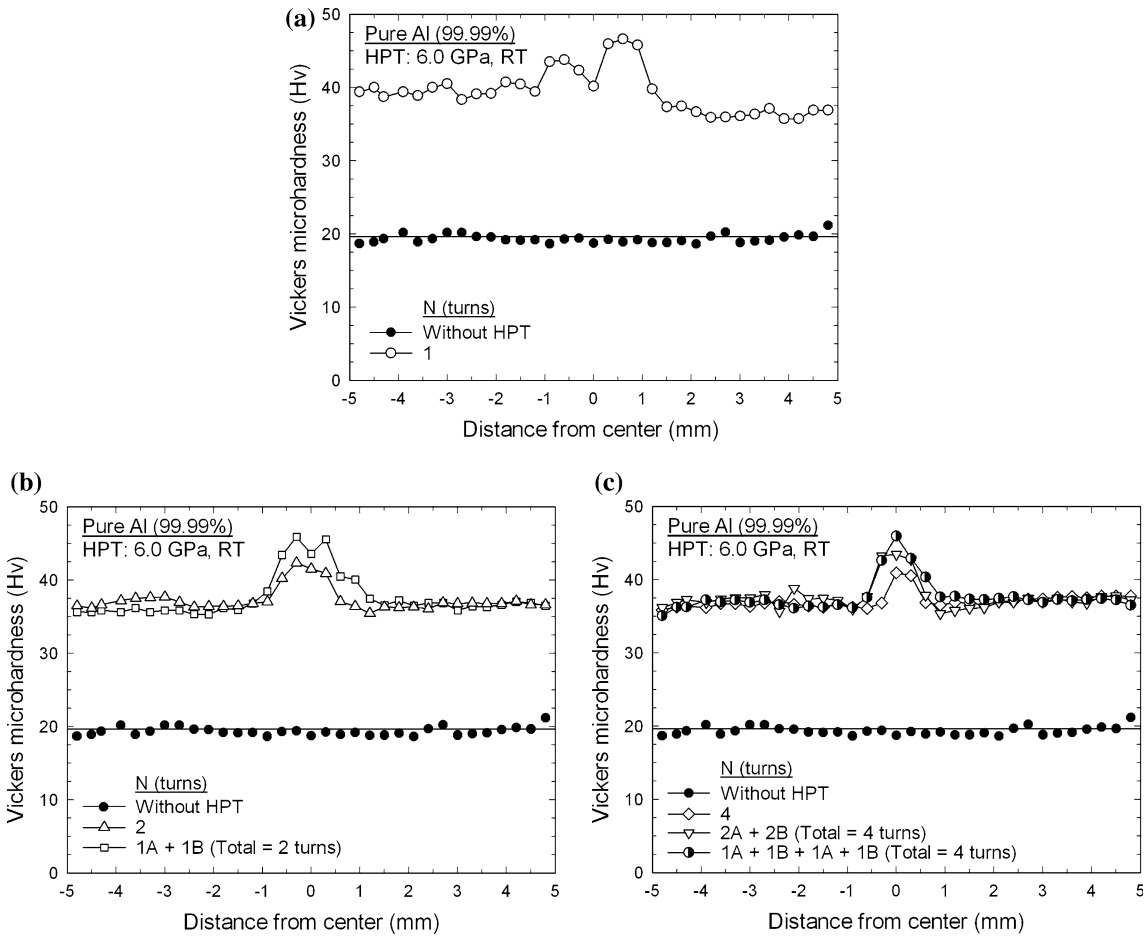

Fig. 1 Variation of Vickers microhardness with position on the disk for samples processed by HPT through **a** one turn, **b** two turns by m-HPT and c-HPT, and **c** four turns by m-HPT and c-HPT: the *lower solid points* denote the unprocessed annealed condition

the disks remain essentially constant at Hv ≈ 36–37 for totals of two and four turns in both the m-HPT and c-HPT conditions as shown in Fig. 1b, c.

Second, the central regions record consistently higher values of Hv, up to >40, in the disks processed by HPT, whereas the values of Hv at the outer peripheries are consistently lower at Hv ≈ 36–37.

Third, in m-HPT the values of Hv in the central region tend to decrease with increasing numbers of turns, whereas there is no clear difference in the Hv values with increasing numbers of total HPT turns in the central regions of the disks after c-HPT. Specifically, in conventional m-HPT there are higher hardness values recorded in the central regions of the disks but there is a gradual evolution with increasing strain toward a reasonably homogeneous distribution of hardness values in the disks at larger strains. Thus, these central regions of higher hardness extend through decreasing areas as the numbers of turns increases. It was reported earlier that the higher values of Hv in the centers of the disks essentially disappear in high-purity Al disks after HPT through five turns [28], whereas very recent results show that in the earliest stages of processing, through a fractional revolution of 1/8 turn, higher hardness values are recorded at the edges rather than in the centers of high-purity Al disks processed by HPT [29, 30]. The present testing was discontinued after four turns where there remains a small region of higher hardness in the disk center but nevertheless these results are consistent with the earlier reports showing the development of reasonable hardness homogeneity. It is relevant to note also that, whereas commercial purity metals and metallic alloys normally have lower hardness values in the centers of the disks compared with the surrounding areas [17, 27, 31–51], a Zn–22%Al eutectoid alloy is the only material to date to show higher hardness values in the centers of the disks, as in high-purity Al, but with all measured hardness values lower than in the annealed condition [52].

Fourth, although the variations in Hv are similar within the central regions for all disk samples after HPT, there is a consistent trend for higher values after c-HPT by comparison with m-HPT and the highest hardness is recorded in the disk subjected to three strain reversals in the 1A + 1B + 1A + 1B condition where the value of Hv is ~46 as shown in Fig. 1c.

Fifth, the central core regions of inhomogeneously higher hardness extend over a significant distance across the diameter after both m-HPT and c-HPT but there is a slightly larger width for the area with inhomogeneous hardness after c-HPT than after m-HPT at the same total number of turns. For example, inhomogeneous core regions extending over ~1.0 and ~0.5 mm are observed after HPT for two and four turns in the m-HPT condition, respectively, whereas the region of higher hardness extends over a central core region of ~1.5 mm in the c-HPT condition for 1A + 1B in Fig. 1b and over ~1.0–1.2 mm for 2A + 2B and 1A + 1B + 1A + 1B for four turns in the c-HPT condition in Fig. 1c.

Microhardness values over the disk surfaces

All of the microhardness data taken from the rectilinear grid patterns were plotted as color-coded three-dimensional mesh plots to provide a pictorial display of the distributions of the individual local hardness after processing by HPT through the different straining conditions. Three-dimensional representations of microhardness were reported earlier for several different materials processed by HPT [33, 44, 50, 53].

The plots are shown in Fig. 2 for the three m-HPT samples in the upper row and the three c-HPT samples in the lower row, where the coordinates X and Y denote two randomly selected perpendicular axes that are superimposed on the disks such that the central point in each disk is given by the coordinates (0, 0). The sets of unique colors filling the plots denote the Hv values from 30 to 60 in incremental steps of 5: the specific values of the various colors are given in the color key on the right in Fig. 2.

The evolution of hardness homogeneity is readily apparent for the m-HPT samples taken through one, two, and four turns in the upper row of Fig. 2. It is apparent that this central region is reduced after two turns and disappears almost completely after four turns, whereas there is a relatively large area of higher hardness in the central region of the disk after one turn. For the disks processed through c-HPT, shown in the lower row of Fig. 2, the central region of higher hardness is well defined after processing in the 1A + 1B condition in Fig. 2d and, in addition, the area of higher hardness is significantly larger in this sample than the central region for the sample tested through m-HPT for two turns in Fig. 2b. After HPT in the 2A + 2B condition in Fig. 2e, the central region displays similar local hardness distributions to the sample processed through two turns in m-HPT in Fig. 2b and again this central region is large by comparison with the central region after m-HPT for four turns in Fig. 2c. The sample tested through 1A + 1B + 1A + 1B has likewise a significantly wider central region of high hardness than either the m-HPT disk taken through four turns in Fig. 2c or the 2A + 2B disk in Fig. 2e. These results demonstrate that the hardened central region is preferentially retained during c-HPT and this retention becomes more effective when the total numbers of cycles is higher as in the 1A + 1B + 1A + 1B condition. It is reasonable to conclude that systematic reversals in the direction of torsional straining are effective in retaining the regions of higher hardness in the centers of the disks to higher imposed strains.

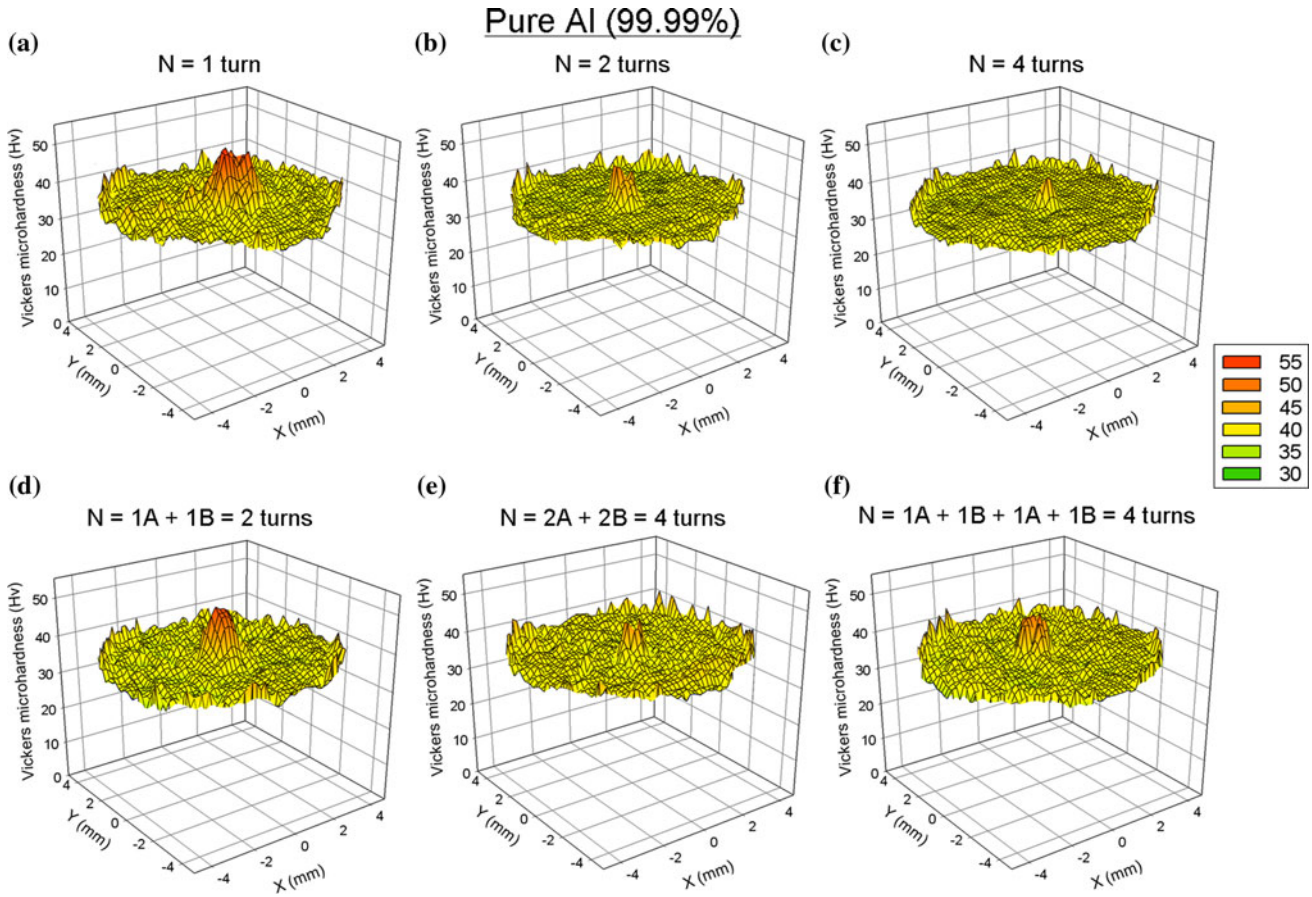

Fig. 2 Color-coded three-dimensional mesh plots showing the distributions of Vickers microhardness over the surfaces of each disk: the *upper row* shows disks processed by m-HPT for **a** one turn, **b** two turns, and **c** four turns and the *lower row* shows disks processed by c-HPT for **d** 1A + 1B, **e** 2A + 2B, and **f** 1A + 1B + 1A + 1B conditions

Microstructural observations after HPT

Microstructural observations were conducted on all disks processed both in the m-HPT and the c-HPT conditions and representative microstructures for these two conditions are displayed in Figs. 3 and 4, respectively. In each disk, the microstructures were recorded at positions near the centers at $r \approx 0$ mm shown in the left columns in Figs. 3 and 4 and at $r \approx 3.5$ mm closer to the edges of the disks shown in the right columns in Figs. 3 and 4. Using Eq. 1, the equivalent strains imposed at $r \approx 3.5$ mm are calculated as $\sim$17.6, $\sim$35.3, and $\sim$70.5 after HPT through totals of one, two, and four turns, respectively. In practice, the measured disk heights after HPT were in the range from 0.70 to 0.73 mm and the calculations of equivalent strain used an average value of $h \approx 0.72$ mm. It should be noted also that the microstructures recorded at $r \approx 3.5$ mm are essentially the closest possible distance from the edges of the disks because of the geometrical restrictions inherent in sample preparation for TEM. All of the micrographs displayed in Figs. 3 and 4 were taken using the same magnification to provide a direct comparison of the evolutions of the local microstructures after HPT processing through different conditions.

Figure 3 shows the microstructures in the disks processed by m-HPT for $N = 1$, 2, and 4 turns at $r \approx 0$ mm on the left and at $r \approx 3.5$ mm on the right. After HPT for one turn, the grain boundaries are obscure, the grains are insufficiently equiaxed and many dislocations exist within the grains at $r \approx 0$ mm in Fig. 3a, whereas there are well-defined boundaries and reasonably equiaxed grains at $r \approx 3.5$ mm in Fig. 3b. After an additional revolution in the same torsional direction to give two turns, there remain many dislocations within the grains at $r \approx 0$ mm such that the microstructure in Fig. 3c is similar to Fig. 3a. Similarly, the microstructure in the disk at $r \approx 3.5$ mm in Fig. 3d is similar to the microstructure after one turn in Fig. 3b. By contrast, after m-HPT for four turns the grain boundaries are clearly observed and the grains are reasonably equiaxed at $r \approx 0$ mm in Fig. 3e and the microstructure at $r \approx 0$ mm is now similar to the microstructure in the same disk at $r \approx 3.5$ mm in Fig. 3f. These

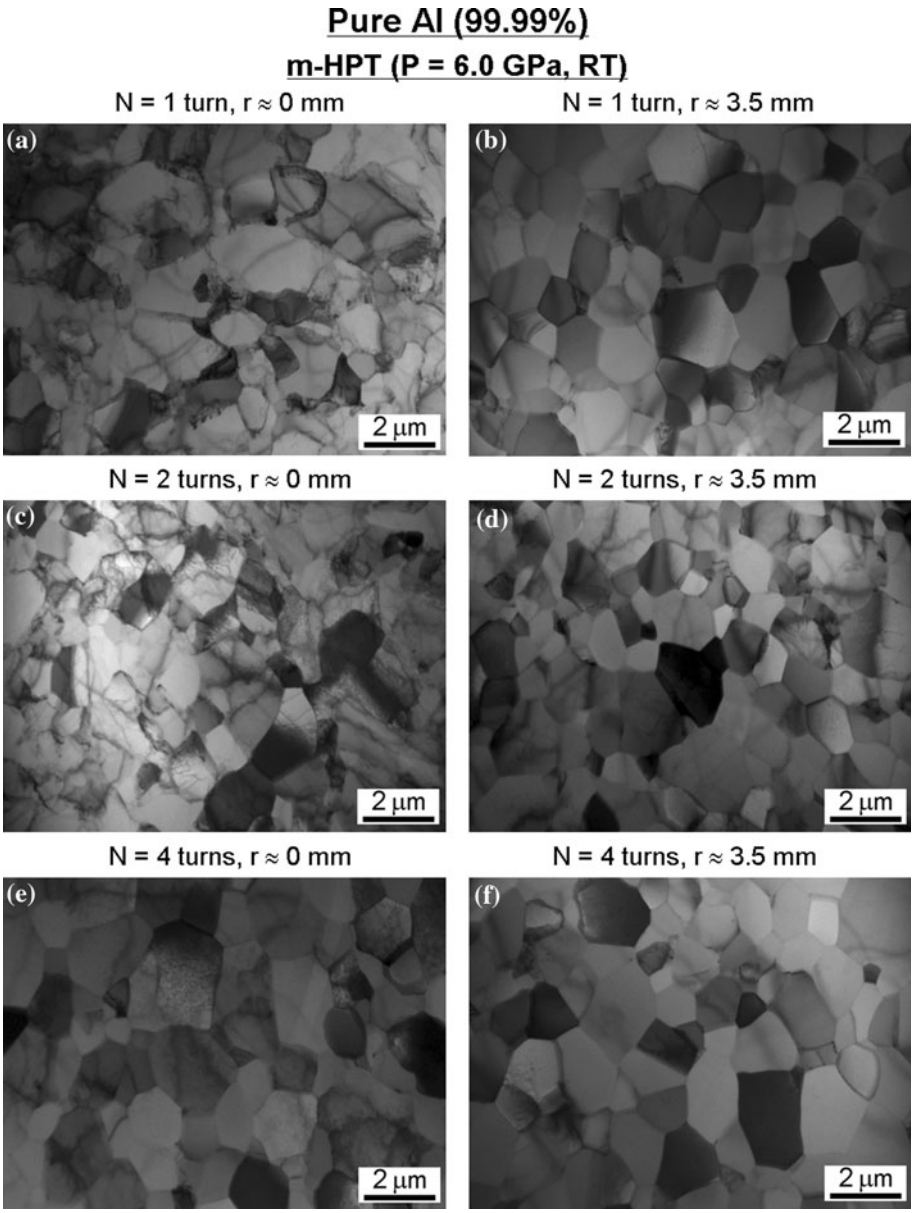

Fig. 3 Representative microstructures for disks processed by m-HPT for one, two, and four turns: the positions at $r \approx 0$ mm are shown in (**a**), (**c**), and (**e**) and the positions at $r \approx 3.5$ mm are shown in (**b**), (**d**), and (**f**)

observations confirm that there is a significant level of microstructural evolution in the disk after m-HPT in the position at $r \approx 0$ mm with increasing numbers of turns up to four turns and, furthermore, the final microstructures after four turns are similar in both the $r \approx 0$ mm and the $r \approx 3.5$ mm positions. Since the grain size is related to the hardness of materials, the evolution of microstructural homogeneity after four turns in m-HPT leads to a reasonably homogeneous local hardness across any diameters and this is consistent with the results shown in Fig. 2c.

The microstructures recorded in the disks processed by c-HPT are shown in Fig. 4 for the 1A + 1B, 2A + 2B, and 1A + 1B + 1A + 1B conditions for totals of two, four, and four turns, respectively, with $r \approx 0$ mm in the left column and $r \approx 3.5$ mm in the right column. Although these samples were processed by c-HPT, all disks in the position at $r \approx 3.5$ mm show consistent microstructures with equiaxed grains surrounded by distinct grain boundaries after processing through totals of two and four turns shown in Fig. 4b, d, and f. Furthermore, these microstructures are very similar to the disks processed by m-HPT for one, two, and four turns in Fig. 3b, d, and f, respectively. On the other hand, the microstructures in the positions at $r \approx 0$ mm after c-HPT show different characters such that after two turns in the 1A + 1B condition in Fig. 4a the material has many dislocations within the grains and the grain boundaries are indistinct. This microstructure is similar to m-HPT after two passes shown in Fig. 3c but careful measurements show the grains in the c-HPT condition are slightly smaller than in the m-HPT condition. In

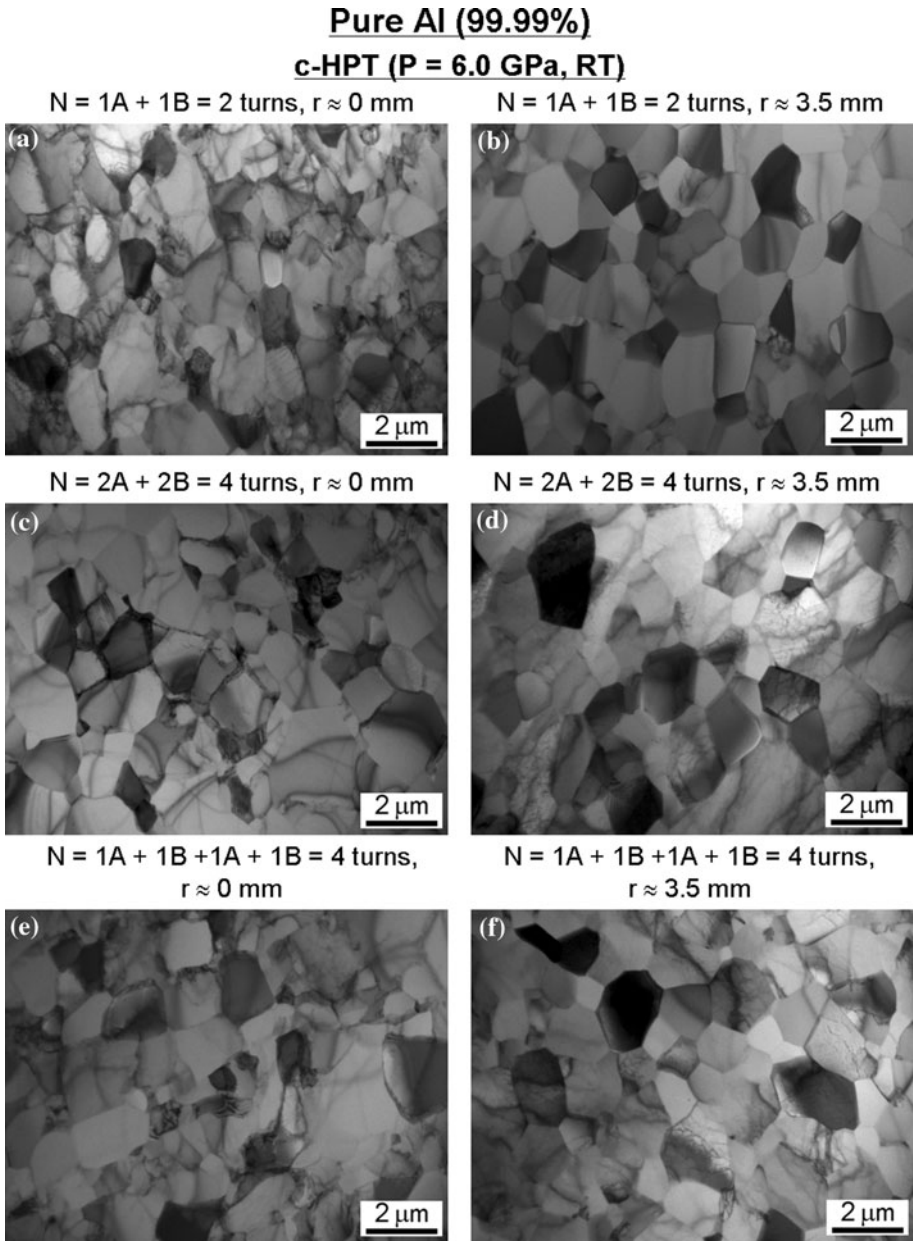

Fig. 4 Representative microstructures for disks processed by c-HPT in the 1A + 1B, 2A + 2B, and 1A + 1B + 1A + 1B conditions: the positions at $r \approx 0$ mm are shown in (**a**), (**c**), and (**e**) and the positions at $r \approx 3.5$ mm are shown in (**b**), (**d**), and (**f**)

addition, at $r \approx 0$ mm after c-HPT for four turns, shown in Fig. 4c, e, there is a higher dislocation density within the grains although the grain sizes are similar to the 1A + 1B condition in Fig. 4a. The general conclusion from these micrographs is that processing through c-HPT produces two different sets of microstructures such that there are equiaxed fine grains and clearly defined grain boundaries at the peripheries of the disks but higher dislocation densities and less well-defined grain boundaries at the centers of the disks. These results demonstrate that the microstructural evolution toward a homogeneous condition, as recorded in the m-HPT samples, will be delayed or possibly even unattainable when using the c-HPT testing condition.

Grain size measurements after m-HPT and c-HPT

Using the TEM micrographs, the average grain sizes were measured both after m-HPT and after c-HPT in the positions at $r \approx 0$ mm and $r \approx 3.5$ mm and the results are shown in Fig. 5a, b, respectively, where the measured average grain sizes are plotted against the total number of HPT turns. The appropriate values of the equivalent strain are indicated along the top of Fig. 5b for the radius of $r = 3.5$ mm where the estimation uses Eq. 1 with an average disk height of ~ 0.72 mm.

The measurements in Fig. 5 lead to several interesting conclusions.

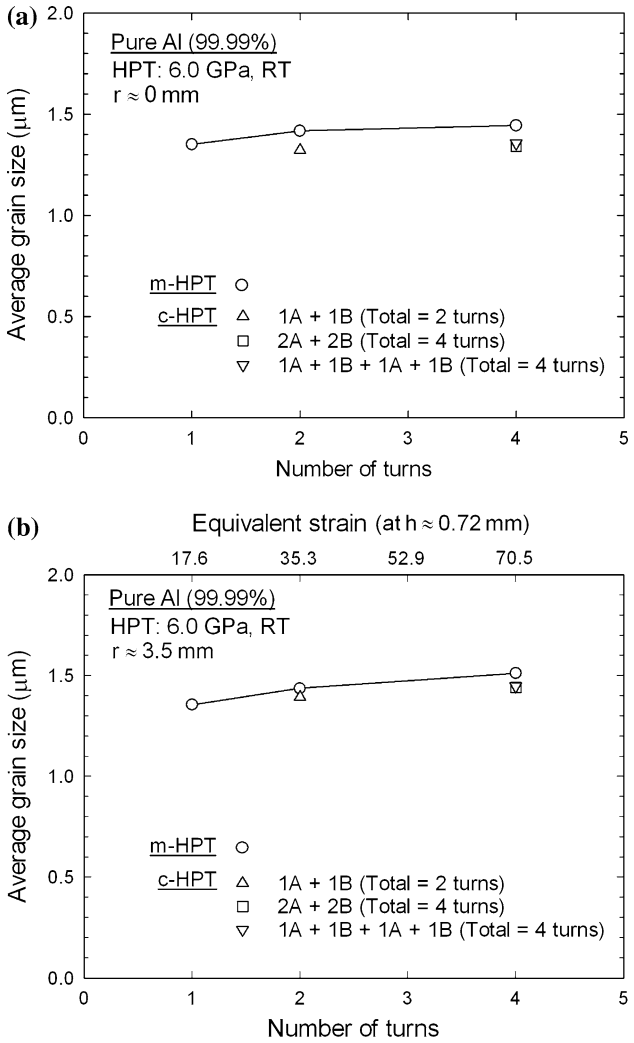

Fig. 5 Average grain size versus number of turns after m-HPT and c-HPT in the positions at **a** $r \approx 0$ mm and **b** $r \approx 3.5$ mm: the estimated equivalent strains are included for each number of total HPT turns in (**b**)

First, at both $r \approx 0$ mm and $r \approx 3.5$ mm the average grain sizes increase slightly with increasing numbers of turns in the disks processed by m-HPT. Detailed inspection shows that the average grain sizes in m-HPT are in the range of $\sim$1.3 to $\sim$1.5 μm at $r \approx 0$ mm, whereas the grain sizes are slightly smaller at $r \approx 3.5$ mm. These results are reasonable because they are consistent with the higher local hardness in the central regions in the disks after m-HPT as shown in Figs. 1a–c and 2a–c.

Second, processing by c-HPT introduces slightly smaller average grain sizes by comparison with the disks processed by m-HPT. This difference is especially clear at the $r \approx 0$ position where the difference is of the order of $\sim$0.1 μm. This result is also consistent with the hardness values since the disks processed by c-HPT have higher hardness values in the central region than after m-HPT at the same number of turns as shown in Fig. 1b, c. The differences in the evolution of microhardness after m-HPT and c-HPT are therefore confirmed both by the microstructural analysis and by the grain size measurements.

Discussion

Hardness and microstructural characteristics

The present results on high-purity Al permit a direct comparison between the evolution of local hardness and the severely deformed microstructures in a series of disks processed under both m-HPT and c-HPT conditions. It is observed that there is a region of high hardness in the centers of the disks after processing by c-HPT and these hardness values are higher than in conventional m-HPT by a factor varying in the range of $\sim$3–8%. Although these differences are relatively small, nevertheless it is a consistent feature for all disks displayed in Figs. 1 and 2. The important conclusion is that, at least under the present experimental conditions for high-purity aluminum, there is evidence that the central region of higher hardness tends to be preferentially retained when samples are subjected to larger values of total strain under cyclic conditions and especially when the strain reversals occur after smaller increments of straining as in the 1A + 1B + 1A + 1B sample. Furthermore, this conclusion is also visible in the microstructures in the form of smaller grains after cyclic straining. These results suggest, therefore, the potential for manipulating the hardness values attained in HPT by using different combinations of strain reversals, where these combinations include both the amount of strain imposed in each rotation and the total numbers of strain reversals imposed on the sample.

There are only a limited number of reports on the grain sizes introduced in high-purity Al after processing by HPT for at least one turn and direct comparisons are also difficult because of uncertainties in the precise positions within the disks where the measurements were taken. Nevertheless, there are reports of grain sizes in high-purity Al of $\sim$1.2 μm near the edge of a disk after one turn at $P = 1.25$ GPa [28], $\sim$2 μm near the edge of a disk after one turn at $P = 1.25$ GPa [30], $\sim$1.9 μm after two turns at $P = 1.0$ GPa [54], and $\sim$1.2 μm at the edges of disks processed using a 24° rotation in both m-HPT and c-HPT and at the intermediate and edge regions of a disk processed using a 96° rotation in both m-HPT and c-HPT [20, 21]. In addition, an average grain size of $\sim$1.5 μm was reported in a ring sample with inner and outer diameters of 14 and 20 mm, respectively, after one turn at $P = 1.0$ GPa [55]. All of these grain size data are consistent with the present results where the measured average grain sizes

were in the range of ~1.3–1.5 μm after HPT through totals of one to four turns using both m-HPT and c-HPT. Since the present tests were extended to a total of four turns, it is concluded that the grains are reasonably stable even when the straining is extended to a high number of repetitive turns. It should be noted that this is also consistent with the results for high-purity Al processed by ECAP where the ultrafine grains were stable up to 8 passes but there was evidence for dynamic recovery and grain growth when pressing through 12 passes [56].

A comparison with earlier results obtained under c-HPT conditions

It is appropriate to compare the present results with earlier data where HPT processing was conducted under cyclic conditions: a summary of all of the results is given in Table 1.

Cyclic HPT was applied to Armco iron and nickel to impose maximum equivalent strains at $r = 3$ mm of 64 and 256, respectively, using a series of different strain increments [22]. In both materials, the microstructures reflected the magnitudes of the strain increments such that at larger increments of straining there was a smaller structure size. For these experiments a smaller structure was produced in the material processed by conventional monotonic HPT. A similar result was reported also for commercial purity Ti [27]. High-purity Al was processed in c-HPT at $P = 5$ GPa for maximum rotations of 24° and 96° to give total equivalent strains at the edge of the disks of ~2 and ~8, respectively, with fixed strain increments having an amplitude of ±12° [20]. These equivalent strains are very small in comparison with the present experiments where the equivalent strains at the edges of the disks were ~25 and ~50 after one and two turns, respectively. Nevertheless, the results at these very low strains showed that at the edges of the disks the average grain size was ~0.1 μm larger after c-HPT than after m-HPT. Although this latter result is consistent with the data for Armco iron and Ni [22] and Ti [27], none of these results are consistent with the present investigation where, as shown in Table 1, c-HPT leads consistently to slightly smaller grain sizes and slightly higher values of hardness within the central region.

To obtain an understanding of this apparent discrepancy, it is necessary to adopt a procedure proposed in early experiments on HPT where it was shown that the various microhardness values may be unified across the HPT disk by plotting against the local equivalent strain [34]. An earlier analysis demonstrated that this approach leads to two different possible relationships between hardness and equivalent strain [52]. Figure 6 shows a schematic illustration of the variations of hardness with equivalent strain (a) for most pure metals and metallic alloys where there is no significant recovery and the hardness increases to a plateau which represents the saturation value and (b) for high-purity Al where the stacking faulty energy is very high so that recovery occurs relatively easily by cross-slip [28] and there is a bell-shaped curve which initially increases, then decreases, and again attains a saturation level. This same approach can be used in the present experiments.

The relationship for the equivalent strain was given earlier as Eq. 1. It should be noted this relationship neglects the additional strain produced by the applied compressive pressure, P, which has been shown experimentally to

Table 1 Data obtained on HPT disks under cyclic conditions

Material	Size of c-HPT structure relative to m-HPT structure	Investigators
Armco iron	Larger	Wetscher and Pippan [22]
Ni	Larger	Wetscher and Pippan [22]
Ti	Larger	Todaka et al. [27]
High-purity Al	Larger	Orlov et al. [20]
High-purity Al	Smaller	This investigation

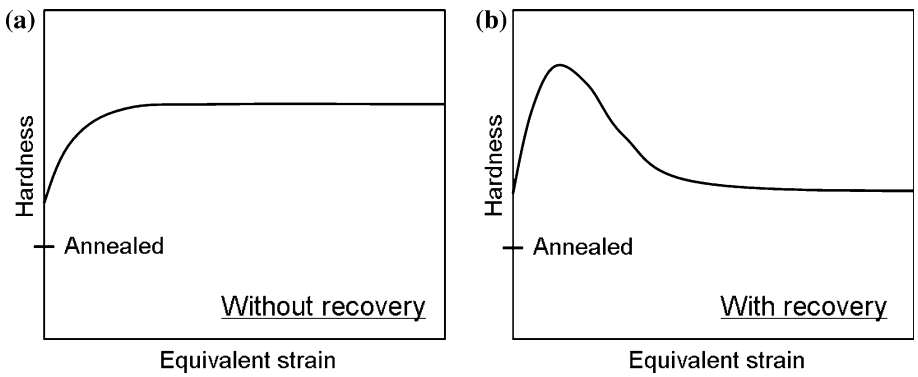

Fig. 6 Schematic illustration of hardness versus equivalent strain for metals processed by HPT **a** without recovery and **b** with recovery: the typical level of the unprocessed annealed condition is indicated [52]

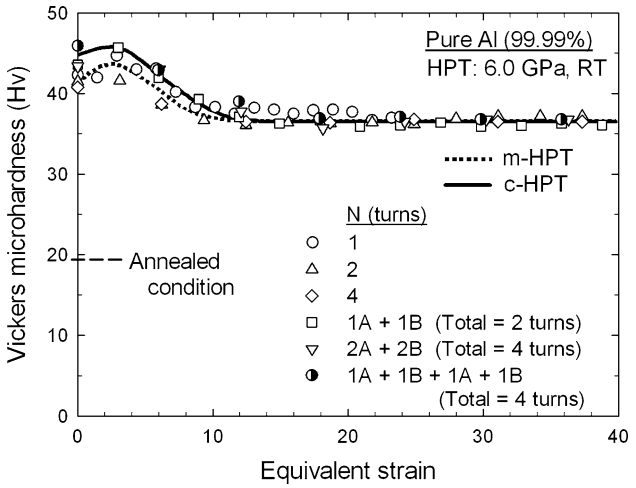

Fig. 7 Vickers microhardness plotted against the calculated equivalent strain for the six straining conditions of m-HPT and c-HPT: the level for the unprocessed annealed condition is indicated

produce straining even in the absence of any torsional rotation [44]. In practice, this additional strain can be neglected because all disks in the present experiments were processed using the same applied pressure of $P = 6.0$ GPa. Therefore, the equivalent strains were calculated using Eq. 1 for each disk and the hardness datum points in Fig. 1 were replotted as the Vickers microhardness against the equivalent strain as shown in Fig. 7 where the initial annealed condition is indicated by a broken line on the vertical axis. To make these calculations, it is noted that all experimental disks had average initial thicknesses close to $\sim$0.80 mm but the thicknesses were reduced to different values during processing where these values were influenced both by the precise initial thickness and by the processing conditions. In the present experiments, the measured reduced thicknesses were $\sim$0.75 mm in the disk after one pass, $\sim$0.70 mm in the disks after two and four passes by m-HPT, $\sim$0.73 mm in the disks after testing through the 1A + 1B and 1A + 1B + 1A + 1B conditions, and $\sim$0.72 mm in the disk after testing through the 2A + 2B condition in c-HPT. These measured experimental values were used as the value for h in order to calculate, using the appropriate values of N and r, the equivalent strains for each separate disk.

Figure 7 shows that the various datum points fall onto two separate curves which are delineated by dotted or solid lines for the materials processed by m-HPT or c-HPT, respectively. Both curves show a similar variation with strain wherein the hardness increases and reaches a maximum value at a small strain and then decreases and ultimately saturates at a lower level at reasonably high strains. It is apparent that the saturation level is identical for both m-HPT and c-HPT processing but the variation at the very lowest strains is different. Both curves in Fig. 7 are in good agreement with the conventional variation in hardness for high-purity Al in m-HPT [29, 30], thereby showing there is a tendency to achieve a saturated hardness after a sufficient total number of turns even for the material processed by c-HPT. Nevertheless, the analysis shows that the hardness values after c-HPT are slightly higher than in m-HPT in the region of small strains which relates to the local area close to the central region in the disk. No error bars are included in Fig. 7 to avoid obscuring the various points and the curves. However, it should be noted that the error bars are very small and the difference between the curves for m-HPT and c-HPT is fully consistent with the microstructural results shown in Fig. 5.

To understand the apparent discrepancy between the present results and those reported in earlier studies using c-HPT with Armco iron and Ni [22], Ti [27], and high-purity Al [20], it is necessary to consider the effect of introducing a strain reversal during HPT. When the direction of straining is reversed, the dislocations introduced during straining in the initial direction will flow back from the dislocation pile-ups so that the total strain introduced in cyclic straining will be slightly less than in conventional monotonic straining where there are no strain reversals. For a material such as high-purity Al where the variation of hardness with equivalent strain follows the bell-shaped curve in Fig. 6b, the reduced strains in the c-HPT samples lead generally, at sufficiently high levels of strain, to higher values of hardness and slightly smaller grain sizes. For Armco iron and Ni [22] and Ti [27], there is only limited recovery and the hardness varies with strain as in Fig. 6a so that the reduced strain in c-HPT will give, as reported experimentally, a lower hardness and a larger grain size. For the earlier experiments on high-purity Al [20], the cyclic strain increments had amplitudes of only $\pm 12°$ so that these experiments were conducted in the very early stages of the bell-shaped curve in Fig. 6b where the hardness increases with equivalent strain: this situation is equivalent to the higher hardness values observed around the periphery of a disk of high-purity Al processed through only 1/8 turn under monotonic conditions [30]. Thus, at these very small strains it is again reasonable to anticipate a lower hardness and a larger grain size in c-HPT.

It follows from this analysis that all of the experimental results reported to date are mutually consistent. However, it is very important to recognize that the variation of hardness with equivalent strain is dependent upon the degree of recovery within the material as depicted schematically in Fig. 6. Therefore, the results obtained by HPT under cyclic conditions for a material exhibiting rapid recovery, such as high-purity aluminum, will depend upon whether the strain reversals are undertaken before or after the peak in hardness with equivalent strain shown in Fig. 6.

Summary and conclusions

1. High-purity aluminum was processed by HPT under m-HPT and c-HPT conditions. Values of the Vickers microhardness were recorded across the diameters and over the surfaces of the disks and the deformed microstructures were investigated using TEM.
2. All disks show higher hardness values in the center regions of the disks and lower values at the edges. Processing by c-HPT produces higher hardness in the central region than m-HPT for the same total number of turns. Microstructural observations and grain size measurements are in excellent agreement with the hardness data. Slightly smaller grain sizes are observed in c-HPT by comparison with m-HPT.
3. The microhardness values correlate with the estimated values of the equivalent strain. The results are consistent with earlier data reported under c-HPT conditions when it is recognized that the variation of hardness with equivalent strain depends both upon the level of recovery within the material and upon whether the strain reversals are undertaken before or after the peak hardness for materials exhibiting rapid recovery.

Acknowledgement This study was supported by the National Science Foundation of the United States under Grant No. DMR-0855009.

References

1. Valiev RZ, Islamgaliev RK, Alexandrov IV (2000) Prog Mater Sci 45:103
2. Valiev RZ, Estrin Y, Horita Z, Langdon TG, Zehetbauer MJ, Zhu YT (2006) JOM 58(4):33
3. Valiev RZ, Langdon TG (2006) Prog Mater Sci 51:881
4. Zhilyaev AP, Langdon TG (2008) Prog Mater Sci 53:893
5. Segal VM, Reznikov VI, Drobyshevskiy AE, Kopylov VI (1981) Russ Metall 1:99
6. Segal VM (1995) Mater Sci Eng A 197:157
7. Furukawa M, Horita Z, Nemoto M, Langdon TG (2001) J Mater Sci 36:2835. doi:10.1023/A:1017932417043
8. Furukawa M, Iwahashi Y, Horita Z, Nemoto M, Langdon TG (1998) Mater Sci Eng A 257:328
9. Furukawa M, Horita Z, Langdon TG (2002) Mater Sci Eng A 332:97
10. Iwahashi Y, Horita Z, Nemoto M, Langdon TG (1997) Acta Mater 45:4733
11. Iwahashi Y, Horita Z, Nemoto M, Langdon TG (1998) Acta Mater 46:3317
12. Bridgman PW (1935) Phys Rev 48:825
13. Bridgman PW (1943) J Appl Phys 14:273
14. Valiev RZ, Ivanisenko YuV, Rauch EF, Baudelet B (1996) Acta Mater 44:4705
15. Wetscher F, Vorhauer A, Stock R, Pippan R (2004) Mater Sci Eng A 387–389:809
16. Wetscher F, Pippan R, Sturm S, Kauffmann F, Scheu C, Dehm G (2006) Metall Mater Trans 37A:1962
17. Horita Z, Langdon TG (2005) Mater Sci Eng A 410–411:422
18. Kawasaki M, Langdon TG (2008) Mater Sci Eng A 498:341
19. Orlov D, Bhattacharjee PP, Todaka Y, Umemoto M, Tsuji N (2008) Mater Sci Forum 584–586:133
20. Orlov D, Todaka Y, Umemoto M, Tsuji N (2009) Mater Sci Eng A 499:427
21. Orlov D, Bhattacharjee PP, Todaka Y, Umemoto M, Tsuji N (2009) Scr Mater 60:893
22. Wetscher F, Pippan R (2006) Philos Mag 86:5867
23. Wetscher F, Pippan R (2009) Metall Mater Trans A 40A:3258
24. Ivanisenko Yu, Fecht HJ (2008) Mater Sci Forum 584–586:203
25. Ivanisenko Yu, Kurmanaeva L, Weissmueller J, Yang K, Markmann J, Rösner H, Scherer T, Fecht HJ (2009) Acta Mater 57:3391
26. Wetscher F, Tian B, Stcok R, Pippan R (2006) Mater Sci Forum 503–504:455
27. Todaka Y, Umemoto M, Yamazaki A, Sasaki J, Tsuchiya K (2008) Mater Trans 49:47
28. Xu C, Horita Z, Langdon TG (2007) Acta Mater 55:203
29. Ito Y, Horita Z (2009) Mater Sci Eng A 503:32
30. Xu C, Horita Z, Langdon TG (2010) Mater Trans 51:2
31. Jiang H, Zhu YT, Butt DP, Alexandrov IV, Lowe TC (2000) Mater Sci Eng A 290:128
32. Zhilyaev AP, Lee S, Nurislamova GV, Valiev RZ, Langdon TG (2001) Scr Mater 44:2753
33. Zhilyaev AP, Nurislamova GV, Kim BK, Baró MD, Szpunar JA, Langdon TG (2003) Acta Mater 51:753
34. Vorhauer A, Pippan R (2004) Scr Mater 51:921
35. Sakai G, Horita Z, Langdon TG (2005) Mater Sci Eng A 393:344
36. Sakai G, Nakamura K, Horita Z, Langdon TG (2005) Mater Sci Eng A 406:268
37. Zhilyaev AP, Oh-ishi K, Langdon TG, McNelley TR (2005) Mater Sci Eng A 410–411:277
38. Yang Z, Welzel U (2005) Mater Lett 59:3406
39. Zhilyaev AP, McNelley TR, Langdon TG (2007) J Mater Sci 42:1517. doi:10.1007/s10853-006-0628-0
40. Ungár T, Balogh L, Zhu YT, Horita Z, Xu C, Langdon TG (2007) Mater Sci Eng A 444:153
41. Todaka Y, Umemoto M, Yin J, Lu Z, Tsuchiya K (2007) Mater Sci Eng A 462:264
42. Balogh L, Ungár T, Zhao Y, Zhu YT, Horita Z, Xu C, Langdon TG (2008) Acta Mater 56:809
43. Xu C, Horita Z, Langdon TG (2008) Acta Mater 56:5168
44. Xu C, Horita Z, Langdon TG (2008) J Mater Sci 43:7286. doi:10.1007/s10853-008-2624-z
45. Todaka Y, Umemoto M, Yamazaki A, Sasaki J, Tsuchiya K (2008) Mater Trans 49:7
46. Harai Y, Kai M, Kaneko K, Horita Z, Langdon TG (2008) Mater Trans 49:76
47. Zhilyaev AP, Gimazov AA, Raab GI, Langdon TG (2008) Mater Sci Eng A 486:123
48. Kai M, Horita Z, Langdon TG (2008) Mater Sci Eng A 488:117
49. Edalati K, Fujioka T, Horita Z (2009) Mater Trans 50:44
50. Xu C, Langdon TG (2009) Mater Sci Eng A 503:71
51. Xu W, Wu X, Figueiredo RB, Stoica M, Calin M, Eckert J, Langdon TG, Xia K (2009) Int J Mater Res 100:1662
52. Kawasaki M, Ahn B, Langdon TG (2010) Acta Mater 58:919
53. Concustell A, Sort J, Woodcock TG, Gimazov A, Suriñach S, Gebert A, Eckert J, Zhilyaev AP, Baró MD (2006) Intermetallics 14:871
54. Edalati K, Ito Y, Suehiro K, Horita Z (2009) Int J Mater Res 100:1668
55. Harai Y, Ito Y, Horita Z (2008) Scr Mater 58:469
56. Kawasaki M, Horita Z, Langdon TG (2009) Mater Sci Eng A 524:143